Quantitative Accuracy Considerations in Dynamic State-of-the-Art PET Imaging (when average counts-per-LOR are (much) less than unity)

Arman Rahmim[1], Ju-Chieh Cheng[2], Stefan Blinder[3], Marie-Laure Camborde[3] and Vesna Sossi[2]
[1]Department of Radiology, Johns Hopkins University School of Medicine, Baltimore, MD
[2]Department of Physics and Astronomy, University of British Columbia, Vancouver, BC
[3]Pacific Parkinson's Research Centre, University of British Columbia, Vancouver, BC

***Abstract*— State-of-the-art high resolution PET is now more than ever in need of scrutiny into the nature and limitations of the imaging modality itself as well as image reconstruction techniques. Particularly, we have discussed and addressed the following two considerations in the context of dynamic PET imaging: (i) The typical average numbers of counts-per-LOR are now (much) less than unity.; (ii) The wide range of statistics (due to physical/biological decay of the activity) coupled with the aforementioned low count-rates-per-LOR further challenge the quantitative accuracy of dynamic reconstructions. In this context, we have argued theoretically and demonstrated experimentally, that the sinogram non-negativity constraint (when using the delayed coincidence and/or scatter subtraction techniques) will result in considerable overestimation biases. Two alternate schemes have been considered, and have been shown to remove the aforementioned bias. We have also investigated applicabilities of ordinary and convergent subsetized image reconstruction methods.**

I. Introduction

In positron emission tomography (PET) systems, there is a continuous effort to increase sensitivity and to improve spatial resolution. The increasing number of LORs in state-of-the-art PET is now beginning to pose challenges from the data storage point of view. Time-complexity of image reconstruction tasks has also become particularly problematic as a consequence. Particularly in dynamic PET imaging, this paper focuses on the following two additional issues: (i) the average number of events per LOR is no longer significantly above unity; (ii) due to the physical and biological decay of the activity distribution, one requires robust and efficient reconstruction algorithms applicable to a wide range of statistics; In the case of the high resolution research tomograph (HRRT), for instance, one typically observes 10-200 M counts per frame (only $\sim$0.012-0.25 average counts per sinogram bin).

It is the very aim of this work to investigate the applicabilities and limitations of various image reconstruction techniques, within the context of state-of-the-art high resolution PET imaging. In particular, we have paid particular attention to the increased likelihood that random coincidences and/or scattered event subtraction methods can yield negative sinogram bins.

II. Random and Scatter Correction Techniques

In the aforementioned context of state-of-the-art dynamic PET imaging, the delayed-coincidence random subtraction technique can introduce challenges to the accuracy of the image reconstruction tasks. Taking the variable Y_i to denote the precorrected counts along a particular LOR i, and defining $\bar{y} = \bar{n}_i + \bar{s}_i$ and $\bar{r}$ as the expected number of randoms-corrected prompts (trues+scatter) and randoms, respectively, Y_i has a distribution given by: $Y = \text{Poisson}\{\bar{y} + \bar{r}\} - \text{Poisson}\{\bar{r}\}$. The Poisson nature of the individual prompts and delayed measurements can subsequently result in negative y_i values. Conventionally, zero-thresholding has been used [1] in order to address divergence issues [2]. The EM algorithm as such can be written as:

$$\lambda_j^{m+1} = \frac{\lambda_j^m}{\sum_{i=1}^{I} p_{ij}} \sum_{i=1}^{I} p_{ij} \frac{[y_i]_+}{\sum_{b=1}^{J} p_{ib}\lambda_b^m + \bar{s}_i} \tag{1}$$

where $[y_i]_+ = y_i$ if $y_i > 0$ and is 0 otherwise, and where λ_j^m denotes the image intensity in voxel j at the mth iteration, and p_{ij} is an element of the probability matrix.

Nevertheless, this approach is bound to result in a positive systematic bias in high resolution tomographs. To see this, we note that Y can be shown [3] to have a probability mass function given by:

$$P(Y = y \mid \bar{y}) = \frac{e^{-(\bar{y}+2\bar{r})}}{i^{|y|}} \left(\sqrt{\frac{\bar{y}+\bar{r}}{\bar{r}}}\right)^y J_{|y|}\left(2i\sqrt{(\bar{y}+\bar{r})\bar{r}}\right) \tag{2}$$

where $J_n(.)$ is the Bessel function of the first kind of order n. Examples of this are depicted in Fig. 1a. With a scanner exhibiting average-counts-per-LOR of $\sim$ 1 (and less), one would expect significant bias to be observed if a sinogram non-negativity constraint is imposed. More quantitatively, defining the percentage bias (PB) as

$$\text{PB} = \left(\frac{\overline{[Y]}_+}{\overline{Y}} - 1\right) \times 100\% \tag{3}$$

Fig. 1b shows plots of the calculated PB for a wide range of random fractions. For average-counts-per-LOR lower than 10, the zero-thresholding effect becomes noticeable. For the typical range of average-counts-per-LOR encountered in a state-of-the-art scanner such as the HRRT (as indicated in the plot), the sinogram non-negativity constraint is then clearly expected to result in an overestimation bias.

A. Sinogram vs. Image Non-negativity Constraints

In order to reduce the systematic bias, we have replaced the sinogram non-negativity constraint with a milder *image*

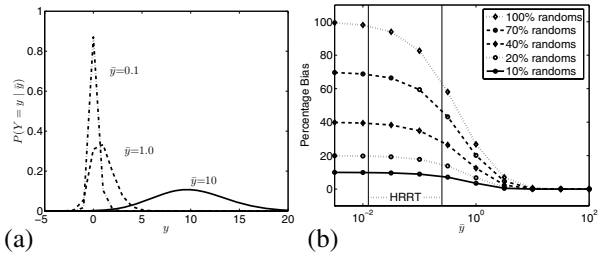

(a) (b)

Fig. 1. (a) The probability $P(Y = y \mid \bar{y})$ as function of y (random fraction is 20%). (b) PB due to zero-thresholding.

non-negativity constraint [4]:

$$\lambda_j^{m+1} = \frac{\lambda_j^m}{\sum_{i=1}^I p_{ij}} \left[\sum_{i=1}^I p_{ij} \frac{y_i}{\sum_{b=1}^J p_{ib} \lambda_b^m + \bar{s}_i} \right]_+ \quad (4)$$

To see how this latter algorithm can significantly reduce the positive bias, let us consider the example of a sphere of diameter D. A single back-projection will typically contribute to a small cylindrical collection of voxels, volume of which is approximately given by $\pi(d/2)^2 D$ (d being the diameter of the tube). For N measured events, then, a voxel receives of the order of M contributions:

$$M = N \frac{\text{Volume of LOR intersection}}{\text{Volume of Object}} = N \frac{\pi \left(\frac{d}{2}\right)^2 D}{\frac{4}{3}\pi \left(\frac{D}{2}\right)^3} = N \frac{3d^2}{2D^2} \quad (5)$$

As an example for the HRRT scanner, using $D = 15$ cm and $d = 2.5$ mm, in a typical accelerated EM reconstruction process ($\sim 10^6$ counts per subset), a voxel inside the object is expected to receive $M \sim 400$ contributions. This is > 3 orders of magnitude larger than the typical average number of counts acquired per sinogram bin in the HRRT, and is therefore expected (Fig. 1) to nearly eliminate the positive systematic bias.

B. Alternative Approach

There are two important advantages in avoiding altogether the delayed-coincidence subtraction technique: *(i)* The subtraction technique increases the variance (noise) of the data. *(ii)* The direct reconstruction of the prompts data does not require any non-negativity constraints. Since the prompts data y_i^p are themselves Poisson distributed, one may maximize an *exact* ordinary Poisson (OP) log-likelihood objective function, using for instance, the OP-EM algorithm [6]:

$$\lambda_j^{m+1} = \frac{\lambda_j^m}{\sum_{i=1}^I p_{ij}} \sum_{i=1}^I p_{ij} \frac{y_i^p}{\sum_{b=1}^J p_{ib} \lambda_b^m + \bar{r}_i + \bar{s}_i} \quad (6)$$

In this work, the expected random rates have been obtained from a generalization [7] of the Casey 3D random-smoothing technique, which first estimates the crystal singles rates from the delayed-coincidence measurements followed by a standard calculation of the random rates from the singles.

C. Scattered Correction

In the aforementioned schemes, two scatter correction techniques have been investigated: *(i) Subtraction of (estimated) scatter in projection-space*: The approach has a potential limitation as it can be seen to be problematic in a very similar sense to the subtraction technique for the delayed coincidences. *(ii) Inclusion of scatter inside the reconstruction algorithm:* Considering, for instance, the OP-EM algorithm (6), the calculated $\bar{s}_i$ values are used in the denominator of the EM algorithm, along with the expected trues and randoms, to provide an expected value for the number of prompts measured along an LOR i. This approach maintains the Poisson nature of the data, and does not require application of non-negativity constraints.

III. Algorithm Implementation and Comparisons

In this work, in addition to the standard histogram-mode EM (HMEM) methods, we have paid particular attention to list-mode EM (LMEM) algorithms. The list-mode approach can result in a number of advantages including: (i) faster reconstructions, (2) preservation of maximum sampling frequency, (3) increased accuracy and convenience in motion correction, as elaborated in [4], [5].

Various accelerated list-mode algorithms have been reviewed in [4], [5]; here we have tested and compared:
(1) Subsetized List-Mode EM (S-LMEM) [similar approach as the histogram-mode OSEM algorithm]
(2) Convergent Subsetized (CS-LMEM) [similar approach as the histogram-mode C-OSEM algorithm]
The following random (and scatter) subtraction techniques:
(1) Sinogram non-negativity (SN) constrained Eq. 1 (histogram-mode only).
(2) Image non-negativity (IN) constrained Eq. 4.
(3) OP-EM algorithm Eq. 6.
were applied to data sets spanning a wide range of statistics.

Specifically, we tested the following:
(i) Schemes without scatter correction:
RS-SN: Random-Subtraction with the SN constraint;
RS-IN: Random-Subtraction with the IN constraint.
(ii) Schemes with scatter correction:
RSS-SN-SC: Random/Scatter-Subtraction with the SN constraint;
RS-IN-SC: Random-Subtraction with the IN constraint; scatter estimates at denominator of EM equation;
OP-(LMEM or HMEM)-SC: random/scatter estimates at denominator of EM algorithm.

IV. Methods and Results

Tomograph: Data were acquired on the second generation of the high resolution research tomographs (HRRT). This HRRT scanner has an octagonal design, with the detector heads consisting of a double 10 mm layer of LSO/LYSO for a total of 119,808 detector crystals (crystal size 2.1 x 2.1 x 10 mm^3).

Experiment – Contrast Phantom: A 20 cm long, 10 cm radius phantom was used. The phantom had two 5 cm diameter cylindrical inserts, one a 'cold' Teflon insert, and the other

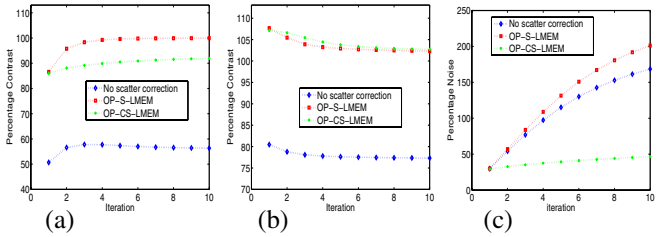

(a) (b) (c)

Fig. 2. Plots of (a) percentage noise, as well as (b) hot and (c) cold contrasts for three reconstruction schemes. The frame included 32M counts.

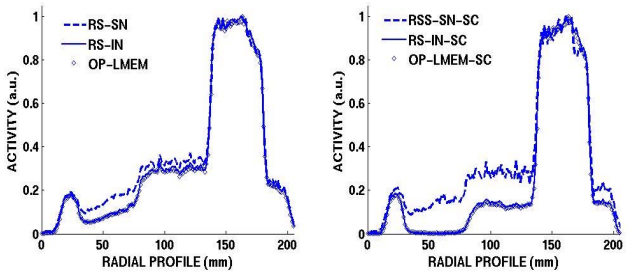

(a) (b)

Fig. 3. Plots of percentage noise (left), as well as hot (middle) and cold (left) contrasts for three reconstruction schemes. The frame included 32M counts.

filled with a ^{11}C radioactivity concentration of 59.4 kBq/ml ('hot' insert). The phantom itself was filled with a ^{18}C concentration of 11.5 kBq/ml ('background'), yielding a hot insert to background ratio of 5.2.

Figs. 2(a,b,c) show plots of percentage noise, as well as hot and cold contrasts for the OP-S-LMEM (with and without scatter correction) and the convergent OP-CS-LMEM algorithms. Clearly, even though the latter scheme relatively suppresses noise, it exhibits a very slow convergence rate in the cold region. We attribute this to the additive nature of the CS-LMEM algorithm [4] resulting in a relatively slow update scheme. Subsequently, we have chosen to use the S-LMEM approach (where applicable) in the rest of this work.

Fig. 3(a) shows transaxial profiles through first frame of the data (161 M total counts, 25% random fraction), reconstructed without scatter correction for the RS-SN, RS-IN and OP-LMEM schemes. Clearly, the sinogram non-negativity constraint (in RS-SN) results in an overestimation bias. On the other hand, use of image non-negativity (in RS-IN) removes this bias with respect to the OP-LMEM technique. In the case when scatter correction is applied, Fig. 3(b) shows radial profiles through images reconstructed using the RSS-SN-SC, RS-IN-SC and OP-EM techniques. Here, we note that the sinogram non-negativity constraint produces an even greater overestimation bias with respect to the OP approach (OP-LMEM or OP-HMEM) (caused by the added effect of scatter subtraction).

Fig. 4(a) shows time-activity curves across 24x5 min frames (spanning 161 M to 3.6 M total counts with randoms fractions ranging from 25% to 5%). Shown in the figure are FORE+2D-FBP and OP-LMEM reconstructions (including scatter correction). The higher level of TAC variance is observed for the

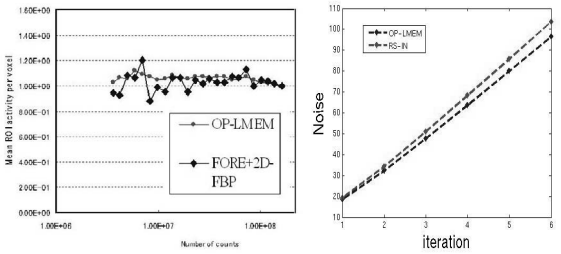

(a) (b)

Fig. 4. Plots of percentage noise (left), as well as hot (middle) and cold (left) contrasts for three reconstruction schemes. The frame included 32M counts.

analytic technique, while the OP technique produces a nearly uniform (non-biased) TAC curve for a very wide range of statistics.

Fig. 4(b) compares the noise properties of the RS-IN (this time with scatter estimation included in the denominator of the EM algorithm) and OP-LMEM algorithms. Clearly, while the IN constraint removes the overestimation bias observed when using the SN constraint, it exhibits a higher degree of noise compared to the OP-LMEM scheme. This is attributed the the exact Poisson nature of the prompts which are directly reconstructed using the OP approach.

V. Conclusion

In this work, we have argued theoretically and demonstrated experimentally that, in the context of state-of-the-art dynamic PET imaging, the sinogram non-negativity constraint can result in a considerable overestimation bias (when using the delayed coincidence and/or scatter subtraction techniques). Subsequently, two schemes were considered: (i) subtraction techniques in which an image non-negativity constraint was imposed. (ii) Implementation of random and scatter estimates inside the reconstruction schemes (direct processing of Poisson-distributed prompts). (i) is able to remove the aforementioned bias as effectively as (ii) [a numerical example was provided explaining this], while (ii), being better conditioned theoretically and involving smoothed randoms, is able to exhibit superior noise characteristics.

References

[1] C. Michel *et al.*, *IEEE NSS/MIC Conf. Record*, vol. 2, pp. 1323, 1998.
[2] S. Ahn *et al.*, *IEEE Trans. Med. Imag.*, vol. 23, pp. 591, 2004.
[3] M. Yavuz, *Ph.D. dissertation*, Univ. Michigan, Ann Arbor, 1999.
[4] A. Rahmim *et al.*, *Phys. Med. Biol.*, vol. 49, pp. 4239-4258, 2004.
[5] A. Rahmim *et al.*, accepted to *Phys. Med. Biol.*, In print, 2005.
[6] D. G. Politte *et al.*, *IEEE Trans. Med. Imag.*, vol. 10, pp. 82-89, 1991.
[7] L. Byars *et al.*, *IEEE Nucl. Sci. Symp. Conf. Record*, 2005.